

# NH–NH Vector Correlation in Peptides by Solid-State NMR

B. Reif,<sup>1</sup> M. Hohwy,<sup>2</sup> C. P. Jaroniec, C. M. Rienstra,<sup>3</sup> and R. G. Griffin<sup>4</sup>

Department of Chemistry and MIT/Harvard Center for Magnetic Resonance, Francis Bitter Magnet Laboratory, Massachusetts Institute of Technology, Cambridge, Massachusetts 02139

Received January 18, 2000; revised March 1, 2000

**We present a novel solid-state magic angle-spinning NMR method for measuring the NH<sub>*i*</sub>–NH<sub>*i+1*</sub> projection angle  $\theta_{i,i+1}$  in peptides. The experiment is applicable to uniformly <sup>15</sup>N-labeled peptides and is demonstrated on the chemotactic tripeptide *N*-formyl-L-Met-L-Leu-L-Phe. The projection angle  $\theta_{i,i+1}$  is directly related to the peptide backbone torsion angles  $\phi_i$  and  $\psi_i$ . The method utilizes the T-MREV recoupling scheme to restore <sup>15</sup>N–<sup>1</sup>H interactions, and proton-mediated spin diffusion to establish <sup>15</sup>N–<sup>15</sup>N correlations. T-MREV has recently been shown to increase the dynamic range of the <sup>15</sup>N–<sup>1</sup>H recoupling by  $\gamma$ -encoding, and permits an accurate determination of the recoupled NH dipolar interaction. The results are interpreted in a quasi-analytical fashion that permits efficient extraction of the structural parameters.** © 2000 Academic Press

**Key Words:** magic angle spinning (MAS) solid-state NMR; dipolar vector correlation;  $\gamma$ -encoded heteronuclear recoupling and homonuclear decoupling; T-MREV; structure determination in peptides.

## INTRODUCTION

In recent years, solid-state magic-angle spinning (MAS) NMR has made important contributions to structure elucidation of biological macromolecules primarily through measurements of internuclear distances (1). Initially, application of rotational resonance (R<sup>2</sup>) experiments (2, 3) to bacteriorhodopsin (4–6) and enzyme–inhibitor complexes (7) provided information about reactive intermediates and the active site of these large proteins not accessible with other spectroscopic techniques. Subsequently, homonuclear experiments were employed together with a collection of specifically <sup>13</sup>C-labeled molecules to successfully constrain the conformation of fibrillar fragments of  $\beta$ -amyloid (8, 9). Similarly, heteronuclear REDOR experiments (10) were used successfully to address the conformation of inhibitors bound to large soluble proteins (11–13).

Structures can also be constrained by measuring the relative

<sup>1</sup> Present address: Institute for Organic Chemistry and Biochemistry, Technical University of Munich, D-85746 Garching, Germany.

<sup>2</sup> Present address: Institute for Molecular Biology and Biophysics, ETH Honggerberg, CH-8093, Zürich, Switzerland.

<sup>3</sup> Present address: Department of Chemistry, Columbia University, New York NY 10027.

<sup>4</sup> To whom correspondence should be addressed. E-mail: [griffin@ccnmr.mit.edu](mailto:griffin@ccnmr.mit.edu) or [rgg@mit.edu](mailto:rgg@mit.edu).

orientation of two interactions around a torsion axis of interest. For example, the relative orientation of two dipolar vectors, two shift tensors, or other combinations such as a shift and dipole tensor can yield directly torsion angles (14, 15). Thus, the relative orientation of <sup>15</sup>N<sub>*i*</sub>–<sup>1</sup>H<sub>*i*</sub> and <sup>13</sup>C<sub>*i*</sub> <sup>$\alpha$</sup> –<sup>1</sup>H<sub>*i*</sub> tensor interactions yields the dihedral angle  $\phi_i$  (16, 17) and the orientation of <sup>15</sup>N<sub>*i*</sub>–<sup>13</sup>C<sub>*i*</sub> <sup>$\alpha$</sup>  and <sup>13</sup>C<sub>*i*</sub><sup>1</sup>–<sup>15</sup>N<sub>*i*</sub> the angle  $\psi_i$  (18, 19) in a peptide backbone. A similar experiment has been employed to examine the side chain torsion angle  $\chi_1$  (20).

Experiments designed to constrain torsion angles may assume a special importance in uniformly <sup>13</sup>C, <sup>15</sup>N-labeled samples. These samples are routinely employed in solution NMR experiments and are appealing for solid-state studies because of their ease of biosynthetic preparation. Nevertheless, in uniformly labeled materials efforts to extract structurally important long distances ( $\sim 4$ – $6$  Å), which exhibit weak dipolar couplings, are complicated by the simultaneous presence of stronger couplings from directly bonded atoms. Specifically, the intensity of a cross peak due to the weak coupling is attenuated by the stronger interactions, an effect referred to as dipolar truncation (21–23). For this reason spectrally selective homonuclear dipolar recoupling techniques (24–27) and also recoupling techniques involving dipolar dephasing to a heteronucleus (28–31) are being developed for distance measurements in multiply labeled samples. In a uniformly <sup>15</sup>N-labeled peptide sample, homonuclear <sup>15</sup>N–<sup>15</sup>N dipolar couplings are all of the same magnitude, and truncation effects do not limit long-range homonuclear polarization transfers.

The experiment described in this publication correlates the orientation of two NH vectors in the peptide backbone of the uniformly <sup>15</sup>N-labeled tripeptide *N*-formyl-L-Met-L-Leu-L-Phe (MLF) (32) illustrated in Fig. 1a. The first 2D increment of the 3D pulse sequence yields a 2D <sup>15</sup>N–<sup>15</sup>N correlation spectrum which may be useful for assigning peptide backbone resonances. In a more general case the experiment yields the projection angle  $\theta_{i,i+1}$  between two neighboring amide NH vectors, a parameter that constrains the backbone torsion angles  $\phi_i$  and  $\psi_i$ . The polarization transfer is achieved by <sup>1</sup>H-driven spin diffusion (33–35). Recently, a similar approach was used to correlate two carbonyl CSA tensors in a polymer (36) and in the protein backbone (37, 38). T-MREV (39) is

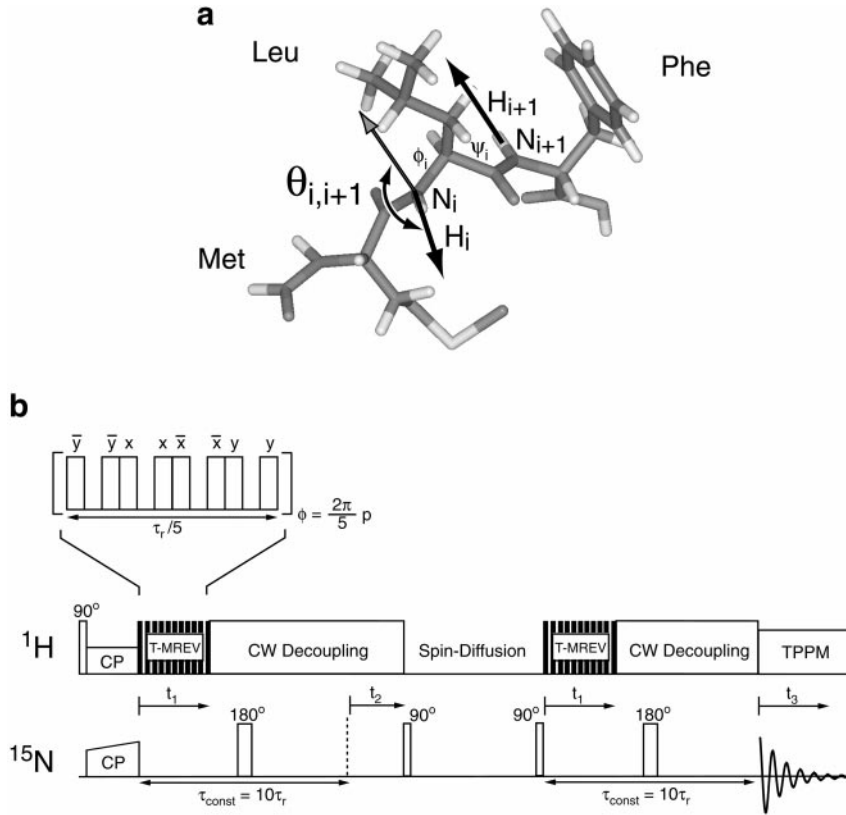


**FIG. 1.** (a) 3D representation of *N*-formyl-L-Met-L-Leu-L-Phe (MLF). The angle  $\theta_{i,i+1}$  corresponds to the projection angle between the two dipolar interactions  $\text{NH}_i$  and  $\text{NH}_{i+1}$ . This angle is directly related to a specific combination of the two backbone angles  $\phi_i$  and  $\psi_i$  in the protein backbone on the Ramachandran diagram. (b) Pulse sequence for the determination of the relative orientation of two NH vectors in the peptide backbone. Chemical shift evolution on nitrogen  $i$  and  $i + 1$  is taking place in  $t_2$  and  $t_3$ , respectively. The NH dipolar coupling is reintroduced simultaneously for nitrogen  $i$  and  $i + 1$  during  $t_1$ . Polarization transfer between the nitrogen nuclei is achieved using proton-mediated spin diffusion. The details of the T-MREV sequence which is used for recoupling of the NH dipolar interaction is given on the top of the pulse sequence.

applied to the  $^1\text{H}$  spins to actively recouple the dipolar interaction in an indirect evolution period while decoupling the  $^1\text{H}$ - $^1\text{H}$  dipolar interactions. The T-MREV sequence is a MREV-8 (40–42)-derived,  $\gamma$ -encoded (43), TC-5-type (44) multiple-pulse sequence that does not refocus the dipolar coupling after each rotor period. The magnitude of the dipolar interaction recoupled by T-MREV does not depend on the powder angle  $\gamma$  which increases the dynamic range of the  $^1\text{H}$ - $^{15}\text{N}$  dipolar recoupling and permits an accurate determination of the projection angle  $\theta_{i,i+1}$ . The dephasing of the nitrogen magnetization depends on the relative orientation of the two  $^{15}\text{N}$ - $^1\text{H}$  dipolar interactions. The data can be analyzed with the projection angle  $\theta_{i,i+1}$  being the sole parameter in a least-squares simulation.

## THEORY

The Hamiltonian operator of the heteronuclear dipolar interaction during MAS can be written as a product of the time-dependent spatial components and the time-independent contributions from the nuclear spin operators

$$H_{\text{IS}}^{\text{D}}(t) = \sum_{\substack{m=-2; \\ m \neq 0}}^{+2} \omega_{0,m}^{\text{IS}} \exp(im\omega_r t) T_{1,0}^{\text{I}} T_{1,0}^{\text{S}}. \quad [1]$$

The definitions for the irreducible tensor operators of rank 1 for spins I and S are

$$\begin{aligned} T_{1,0}^{\text{I}} &= I_z, & T_{1,0}^{\text{S}} &= S_z \\ T_{1,\pm 1}^{\text{I}} &= \mp \frac{1}{\sqrt{2}} I^{\pm}, & T_{1,\pm 1}^{\text{S}} &= \mp \frac{1}{\sqrt{2}} S^{\pm}. \end{aligned} \quad [2]$$

In the following I and S represent  $^1\text{H}$  and  $^{15}\text{N}$  spins, respectively. The spatial components  $\omega_{0,m}^{\text{IS}}$  can be represented as

$$\omega_{0,m}^{\text{IS}} = -2b_{\text{IS}} D_{0,-m}^2(\Omega_{\text{PR}}) d_{-m,0}^2(\beta_{\text{RL}}), \quad [3]$$

where  $b_{\text{IS}}$  is the dipole–dipole coupling constant

$$b_{\text{IS}} = \frac{\gamma_I \gamma_S \hbar}{r_{\text{IS}}^3} \frac{\mu_0}{4\pi}. \quad [4]$$

The coefficients  $D_{0,m}^2(\Omega_{\text{PR}})$ ,  $\Omega_{\text{PR}} = \{0, \beta_{\text{PR}}, \gamma_{\text{PR}}\}$ , are the Wigner rotation matrices that define the coordinate transformation from the principal axis frame to the rotor frame.  $\beta_{\text{PR}}$  and  $\gamma_{\text{PR}}$  are the polar and azimuthal angles, respectively, specifying the orientation of the molecular frame dipolar coupling tensor to the rotor-fixed frame. The transformation from the rotor frame to the laboratory frame is achieved by a subsequent rotation by the magic angle of  $\beta_{\text{RL}} = \tan^{-1}\sqrt{2}$ . The Wigner matrices are given by

$$D_{0,m}^2(\Omega_{\text{PR}}) = d_{0,m}^2(\beta_{\text{PR}}) \exp(-im\gamma_{\text{PR}}), \quad [5]$$

where the reduced Wigner matrix elements  $d_{0,m}^2(\beta)$  are defined as

$$\begin{aligned} d_{0,0}^2(\beta) &= \frac{1}{2}(3 \cos^2\beta - 1) \\ d_{0,\pm 1}^2(\beta) &= \pm \sqrt{\frac{3}{8}} \sin(2\beta) \\ d_{0,\pm 2}^2(\beta) &= \sqrt{\frac{3}{8}} \sin^2\beta. \end{aligned} \quad [6]$$

RF irradiation is incorporated into this treatment via application of the Wigner matrix elements  $D_{\mu,0}^1(\Omega_{\text{RF}})$  to the irreducible tensor operator  $T_{1,0}^1 T_{1,0}^S$  (3, 45)

$$\begin{aligned} U_{\text{RF}}^\dagger(t) T_{1,0}^1 U_{\text{RF}}(t) &= \sum_{\mu} D_{\mu,0}^1[\Omega_{\text{RF}}(t)] T_{1,\mu}^1 \\ &= \sum_{\mu} d_{\mu,0}^1[\beta_{\text{RF}}(t)] e^{-i\mu\alpha_{\text{RF}}(t)} T_{1,\mu}^1, \end{aligned} \quad [7]$$

where  $\alpha_{\text{RF}}$  and  $\beta_{\text{RF}}$  denote the time-dependent RF phase and spin rotation angle of the pulses, respectively. The overall phase of the pulse sequence in each element is included by multiplication with a phase factor  $\exp[-i\mu\phi(t)]$ . If the sequence contains  $n$  elements in each rotor cycle, the phase of the  $p$ th element is  $\phi(t) = 2\pi p/n$ . The first-order average Hamiltonian  $\overline{H}^{(1)}$  of an  $n$ -fold symmetric pulse sequence is constructed from  $n$  elements within  $N$  rotor periods<sup>5</sup> and can then be expressed as (22, 46)

$$\begin{aligned} \overline{H}_{\text{IS}}^{(1)} &= \frac{1}{n} \sum_{p=0}^{n-1} \sum_{m=-2}^{+2} \sum_{\mu_1=-1}^{+1} \overline{\omega_{\mu_1,m}^{\text{IS}}} \\ &\times \exp\left[i \frac{2\pi}{n} (Nm - \mu_1)p\right] T_{1,\mu_1}^1 T_{1,0}^S, \end{aligned} \quad [8]$$

<sup>5</sup> In this work we employ the notation used in Ref. (46).

where  $\overline{\omega_{\mu_1,m}^{\text{IS}}}$  gives the amplitude of the interaction frame average Hamiltonian terms of the dipolar coupling between spins I and S

$$\overline{\omega_{\mu_1,m}^{\text{IS}}} = \frac{n}{N\tau_r} \int_0^{n/N\tau_r} d\tau i^{\mu_1} \omega_{0,m}^{\text{IS}} d_{\mu_1,0}^1[\beta_{\text{RF}}(\tau)] e^{i\mu\alpha_{\text{RF}}(\tau)} e^{im\omega_r\tau}, \quad [9]$$

where  $N\tau_r/n$  corresponds to the length of one T-MREV cycle. Recoupling can occur only when the spatial components match the spin components of the sequence:

$$Nm - \mu_1 = qn. \quad [10]$$

For the C5 T-MREV experiment used here,  $N$  and  $n$  were chosen to be  $N = 1$  and  $n = 5$ , respectively. This leads to recoupling of the spatial and spin components with  $m = \mu = \pm 1$ . The basic building block of the T-MREV sequence is derived from the MREV-8 (40–42) element. In contrast to the traditional MREV-8 variant where the effective Hamiltonian lies in the  $x$ - $z$  plane, inclined by  $45^\circ$  with respect to the  $z$  axis, the effective precession axis of the Hamiltonian in the T-MREV multiple pulse sequence is located purely in the transverse plane. Furthermore, the basic C5 element is phase-shifted in order to reintroduce the dipolar interaction. To date, no other projection angle experiment using  $\gamma$ -encoded recoupling has been described, where the interaction is not refocused after each rotor period.

The magnitude of the recoupled interaction is given by the product of the amplitude of the spatial component  $\omega_{0,\pm 1}^{\text{IS}}$  and the complex scaling factor  $\kappa$  of the sequence.  $\kappa$  is determined by the symmetry number  $n$  and the details of the elements in the pulse sequence. In the analysis, the theoretical value of  $|\kappa| = 0.5026$  (for  $n = 5$  and  $N = 1$ ) was used (39). However, precise calibration of the experimental scaling factor is not crucial for the description of the  $^{15}\text{N}^1\text{H}$ - $^{15}\text{N}^1\text{H}$  recoupling experiment, since the dipolar dephasing of the correlated peak displays only modest dependence on the scaling of the effective  $^{15}\text{N}$ - $^1\text{H}$  dipolar couplings and strong dependence on their relative orientation.

Since the amplitude of the recoupled interaction is dependent on only the angle  $\beta_{\text{PR}}$ , this type of sequence is referred to as  $\gamma$ -encoded (43). This behavior makes a quasi-analytical treatment of the experiment particularly convenient. Furthermore, the correct dephasing behavior of the coherences is analyzed in our case by accounting for differential relaxation between the states  $S_x$  and  $2S_y I_\gamma$  (39).

Figure 1b illustrates the experiment for correlating two  $^{15}\text{N}$ - $^1\text{H}$  interactions in an indirect dimension yielding the relative orientation between  $N_i\text{H}_i$  and  $N_{i+1}\text{H}_{i+1}$  vectors in the peptide backbone. The basic T-MREV building block used to recouple the  $^1\text{H}$ - $^{15}\text{N}$  heteronuclear interaction is shown above

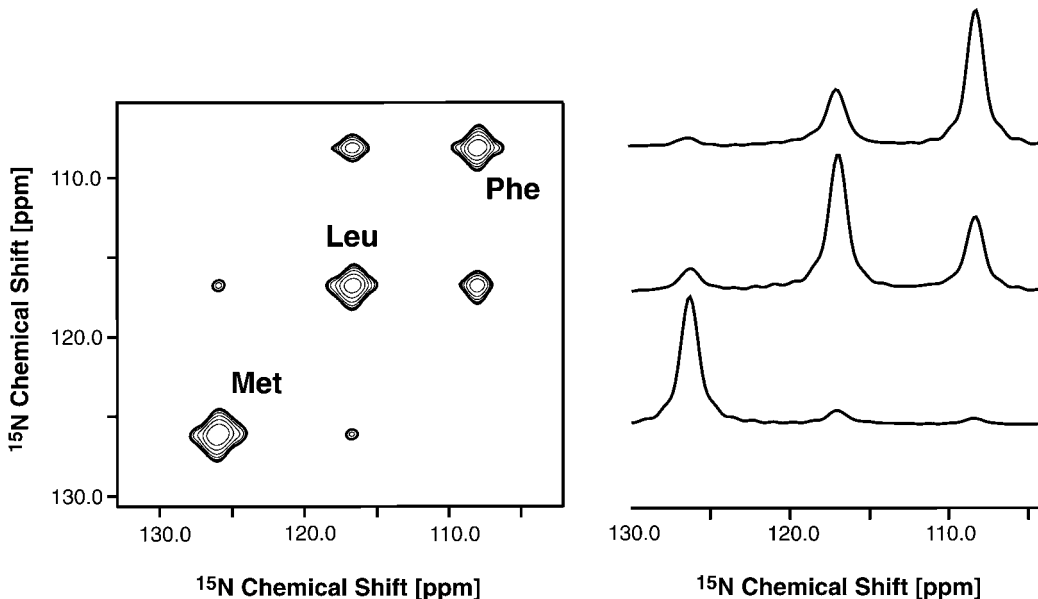


**FIG. 2.** 2D  $^{15}\text{N}$ - $^{15}\text{N}$  correlation spectrum from the 3D pulse sequence depicted in Fig. 1b with  $t_1 = 0$ . The 1D spectra show cross sections through the diagonal and cross peaks in the 2D experiment. The assignment of the resonances is given in the figure.

the first T-MREV element in the pulse sequence. Initially, magnetization is transferred from  $^1\text{H}$  to  $^{15}\text{N}$  by ramped cross polarization. The main building block of the sequence consists of two dipolar dephasing periods  $t_1$  that utilize the T-MREV recoupling sequence to reintroduce the  $^{15}\text{N}$ - $^1\text{H}$  dipolar interaction. The constant time dephasing period uses 10 rotor periods  $\tau_r$  in each element yielding a maximum dephasing time of five rotor periods. Most approaches to this problem are derived from dipolar-chemical shift experiments (48) and use MREV to generate dipolar sideband patterns which permit torsion angles to be constrained (15, 16). In our implementation, T-MREV leads to a heteronuclear dipolar interaction that is not refocused after each rotor period and yields a scaled powder pattern in the dipolar domain. Magnetization is transferred between the  $^{15}\text{N}$  via proton-mediated spin diffusion (33–35).

$^{15}\text{N}$  chemical shift evolution of the nitrogen spins occurs during  $t_2$  and  $t_3$ , respectively. The corresponding 2D  $^{15}\text{N}$ - $^{15}\text{N}$  spectrum, representing the  $t_1 = 0$  plane of the 3D experiment depicted in Fig. 1b, is shown in Fig. 2.

In order to simulate the effects of the sequence, the angle  $\beta^{(2)}$  of the second NH vector is expressed as a function of  $\beta^{(1)}$ , the  $\beta_{\text{PR}}$  angle of the first NH vector, the angle  $\theta_{12}$  between the two vectors, and an angle  $\varphi$  which describes a rotation of the second NH vector around the first on the surface of a cone (Fig. 3):

$$\cos \beta^{(2)} = \cos \beta^{(1)} \cos \theta_{12} - \sin \beta^{(1)} \sin \theta_{12} \cos \varphi. \quad [11]$$

The total signal intensity is the product of the signal intensities during the individual dephasing periods before and after the

mixing time as a function of the  $t_1$  increment for each crystal-lite orientation

$$\begin{aligned} S^{\text{NH}}(t_1, \theta_{12}) &= \int_0^\pi d\beta^{(1)} \sin \beta^{(1)} \int_{-\pi/2}^{+\pi/2} d\varphi S^{\text{NH}}(t_1, \beta^{(1)}, \beta^{(2)}) \\ &= \int_0^\pi d\beta^{(1)} \sin \beta^{(1)} \int_{-\pi/2}^{+\pi/2} d\varphi S^{\text{NH1}}(t_1, \beta^{(1)}) \\ &\quad \times S^{\text{NH2}}(t_1, \beta^{(2)}). \end{aligned} \quad [12]$$

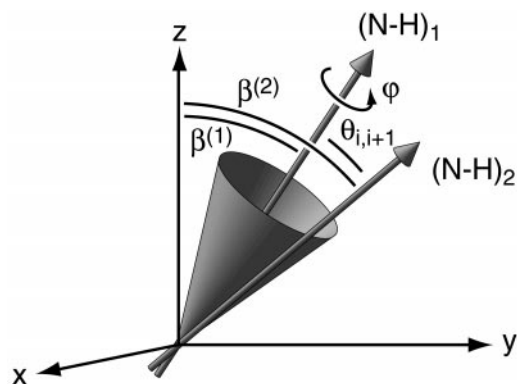


**FIG. 3.** The  $\beta$ -angle of a second dipolar vector  $\beta^{(2)}$  can be expressed as a function of the first dipolar vector  $\beta^{(1)}$ , the angle between the two interactions  $\theta_{i,i+1}$ , and an angle  $\varphi$  which allows for rotations of the second vector around the first NH vector.

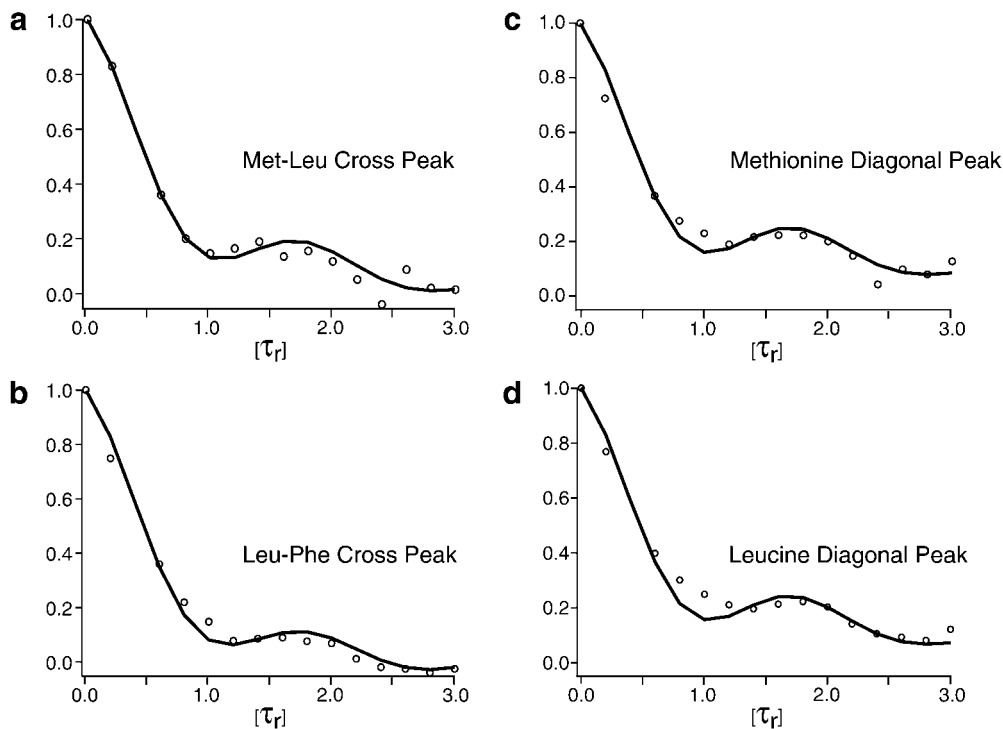


**FIG. 4.** Time domain NH dipolar dephasing spectra for the correlations Met–Leu (a) and Leu–Phe (b) and the diagonal peaks of Met (c) and Leu (d). The projection angle  $\theta_{i,i+1}$  between subsequent NH vectors in the peptide backbone can be determined as  $\theta_{\text{Met,Leu}} = 165^\circ$ ,  $\theta_{\text{Leu,Phe}} = 25^\circ$ . The error was estimated to be less than  $5^\circ$ . The  $x$  axis corresponds to the indirect evolution period  $t_1$  from the pulse sequence shown in Fig. 1b in units of one rotor period. The intensity is normalized to the intensity of the signal in the first increment. Circles and solid lines indicate experimental and simulated data, respectively. The only free parameter in the simulations is the angle  $\theta_{i,i+1}$  between the two NH vectors.

The dephasing of the signal due to the NH dipolar interactions in the two dephasing periods can be written as

$$S^{\text{NH}1/2}(t_1, \beta^{(1/2)}) = \cos \left[ \left| \kappa \right| \frac{b_{\text{IS}}}{2\sqrt{2}} t_1 \sin 2\beta^{(1/2)} \right]. \quad [13]$$

For the second dipolar interaction,  $\beta^{(2)}$  is expressed as a function of  $\beta^{(1)}$  and the angle  $\theta_{12}$  between the two vectors. To account for all possible relative orientations of the two NH vectors, a second integral over the angle  $\varphi$  is evaluated which describes the orientation of the second NH vector around the first on the surface of a cone. Using this approach, the dipolar dephasing spectra acquired with the pulse sequence shown in Fig. 1b can be accurately simulated. The only variable parameter in the simulations is the angle  $\theta_{12}$  between the two NH vectors. The minimum of a least-squares fit directly yields the desired projection angle.

## EXPERIMENTAL

$^{15}\text{N}$ -labeled amino acids methionine, leucine, and phenylalanine were obtained from Cambridge Isotope Laboratories, Inc. (Andover, MA). American Peptide Co., Inc. (Sunnyvale, CA), performed the synthesis of *N*-formyl-MLF. The NMR

spectra were recorded at a  $^1\text{H}$  Larmor frequency of 397.8 MHz, using a custom-designed spectrometer and data acquisition software courtesy of Dr. D. Ruben. The custom-designed triple-resonance transmission line probe was equipped with a 4-mm Chemagnetics/Varian (Fort Collins, CO) MAS spinning module. The spinning frequency was adjusted to 5952 Hz and controlled by a Doty Scientific Inc. (Columbia, SC) spinning frequency controller to within  $\pm 5$  Hz. The  $^1\text{H}$   $90^\circ$  pulse length in the T-MREV multiple-pulse sequence was set to  $2.8 \mu\text{s}$ , to accommodate five MREV cycles in one rotor period. The T-MREV  $^{15}\text{N}$ – $^1\text{H}$  dephasing period in the  $t_1$  evolution period was incremented by  $33.6 \mu\text{s}$  and a total of 16 experiments were recorded in  $t_1$ . In the  $^{15}\text{N}$  chemical shift evolution period  $t_2$ , 24 increments were recorded, with an increment of  $672 \mu\text{s}$  per experiment. The mixing period was set to 3.98 s and the recycle delay between each transient was 4 s. The total experimental time for the 3D experiment was 54 h. CW and TPPM (49) decoupling were used in the indirect and direct evolution periods, respectively, with a  $^1\text{H}$  RF field of about 100 kHz.

Dipolar dephasing determined by the heteronuclear dipolar couplings occurs during  $t_1$ . Figure 4 shows experimental data and simulations for the time domain dephasing of the cross peaks Met–Leu and Leu–Phe (a, b) and the diagonal peaks Met and Leu (c, d) in *N*-formyl-L-Met-L-Leu-L-Phe. The diagonal

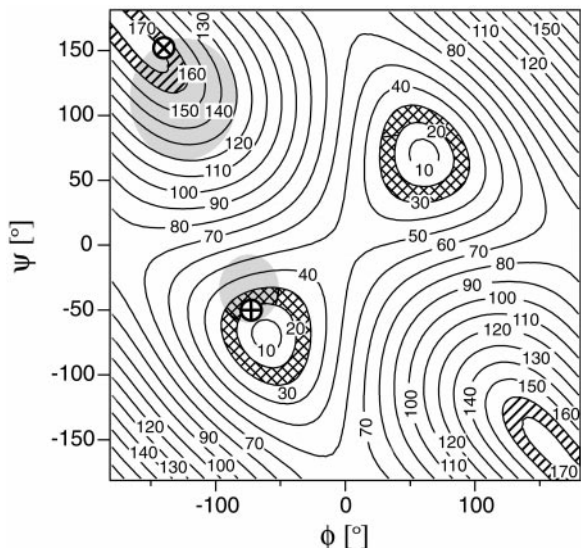


**FIG. 5.** Projection angle between the vectors  $\text{NH}_i$  and  $\text{NH}_{i+1}$  of the amino acid  $i$  and  $i + 1$ , respectively, as a function of the backbone angles  $\phi_i$  and  $\psi_i$  in a protein. Hatched regions indicate combinations of  $\phi$  and  $\psi$  values that are compatible with the NMR spectroscopic data for Met (hatched) and Leu (cross-hatched). Crosses correspond to  $\phi$  and  $\psi$  values found in the X-ray structure of *N*-formyl-MLF-OMe ( $\times$  for Met,  $+$  for Leu). Grey shaded regions indicate  $\beta$ -sheet and  $\alpha$ -helical regions in the Ramachandran diagram.

peaks are included since the dephasing of the signal due to the NH dipolar coupling is analogous to the case of parallel vector orientation and can therefore serve as an internal reference.

## DISCUSSION

Figure 5 shows a plot of  $\theta_{i,i+1}$ , the relative orientation between the two NH vectors of residues  $i$  and  $i + 1$ , as a function of the backbone torsion angles  $\phi_i$  and  $\psi_i$ . The angle  $\theta_{i,i+1}$  depends only on the torsion angles  $\phi_i$  and  $\psi_i$  according to

$$\cos\theta_{i,i+1} = -0.259 \cos\phi_i \cos\psi_i + 0.723 \sin\phi_i \sin\psi_i + 0.471 \cos\phi_i + 0.362 \cos\psi_i + 0.01. \quad [14]$$

A derivation of this formula is provided in the Appendix.

Regions corresponding to  $\alpha$ -helical and  $\beta$ -sheet secondary structure elements are indicated in gray. Fits of the time domain dipolar dephasing signal of the cross peaks yield an angle  $\theta_{i,i+1} = 165^\circ$  for Met-Leu and an angle  $\theta_{i,i+1} = 25^\circ$  for Leu-Phe. The second solution can be excluded in both cases as can be seen from the cross-peak buildup in Fig. 6 (*vide infra*). The hatched regions indicate the possible NMR experimental data in the diagram.  $\theta_{i,i+1}$  is especially sensitive to variation of the backbone angle  $\psi$  in the  $\alpha$ -helical region, whereas in the  $\beta$ -sheet region changes in both backbone angles contribute significantly to changes of  $\theta_{i,i+1}$ . To evaluate the accuracy of the data, we calculated the rms difference between theoretical and experimental data of the time domain dipolar dephasing

curves from Fig. 4 as a function of  $\phi_i$  and  $\psi_i$ . The rmsd diagram for the Leu-Phe cross peak is shown in Fig. 7. Small variations in the backbone angles  $\phi$  and  $\psi$  lead to a significant change in the rmsd values. Furthermore, the dephasing of the diagonal peaks illustrated in Fig. 4 serves as an internal reference for estimating the error on the measured projection angle. For the diagonal peaks, each nitrogen coherence dephases twice under the influence of its NH dipolar coupling during the incremented time period  $t_1$ . The dephasing is therefore analogous to the case of two NH vectors that are oriented parallel to one another, corresponding to  $\theta_{i,i+1} = 0^\circ$  or  $180^\circ$ . This value can be reproduced with an accuracy of better than  $\pm 3^\circ$ . The resolution of the grid was  $1^\circ$  in this case.

The torsion angles determined in this experiment are in good agreement with the data from X-ray crystallographic investigations of *N*-formyl-L-Met-L-Leu-L-Phe-OMe (50). The  $\phi$  and  $\psi$  angles found in the X-ray structure are  $\phi(\text{Met}) = -140.0^\circ$ ,  $\psi(\text{Met}) = 151.3^\circ$ ,  $\phi(\text{Leu}) = -67.7^\circ$ , and  $\psi(\text{Leu}) = -49.3^\circ$ . These are indicated in Fig. 5 with crosses. The values fall onto the respective contour lines found from the NMR experimental data.

It can be seen from Eq. [11]–[13] that the dephasing signal of the projection angle experiment is invariant to the angles  $\theta_{12}$  and  $180^\circ - \theta_{12}$ . In order to differentiate between  $\alpha$ -helical and  $\beta$ -sheet regions in the Ramachandran diagram,  $^{15}\text{N}$ – $^{15}\text{N}$  cross-

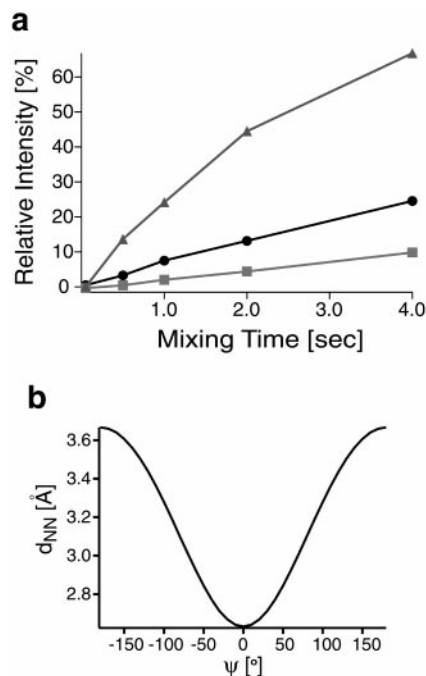


**FIG. 6.** (a) Ratio of cross-peak versus diagonal-peak intensity in the  $^{15}\text{N}$ – $^{15}\text{N}$  spin diffusion experiment as a function of mixing time. The cross peaks between Leu-Phe, Met-Leu, and Met-Phe are coded as triangles, circles, and squares, respectively. (b)  $N_i$ – $N_{i+1}$  distance as a function of the angle  $\psi_i$  in the protein backbone.

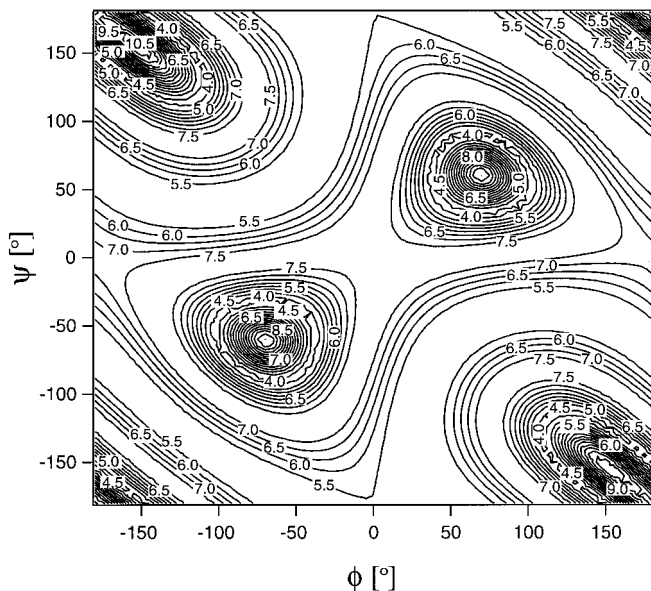


**FIG. 7.** rms difference diagram between experimental and simulated data as a function of the backbone angles  $\phi$  and  $\psi$ . The calculations are carried out for the Leu–Phe cross peak. The lowest rmsd values are obtained for regions in the Ramachandran plot from Fig. 5 where the  $\text{NH}_i\text{--NH}_{i+1}$  projection angle adopts a value of  $25^\circ$  and  $155^\circ$ , respectively.

peak buildup curves were recorded, which provide an estimate of the  $^{15}\text{N}_i\text{--}^{15}\text{N}_{i+1}$  distance.

Figure 6a shows the cross-peak buildup as a function of the spin diffusion time. Clearly, the Leu–Phe cross peak shows a significantly faster buildup rate than the Met–Leu cross peak. Figure 6b shows the  $^{15}\text{N}_i\text{--}^{15}\text{N}_{i+1}$  distance as a function of the backbone angle  $\psi$ . The distance is shorter for  $\alpha$ -helical ( $\psi \approx -30^\circ\text{--}50^\circ$ ) than  $\beta$ -sheet type residues ( $\psi \approx 70^\circ\text{--}150^\circ$ ). This is in agreement with the X-ray structure which gives a value for the  $^{15}\text{N}_i\text{--}^{15}\text{N}_{i+1}$  distance of  $^{15}\text{N}(\text{Met})\text{--}^{15}\text{N}(\text{Leu}) = 3.59 \text{ \AA}$  and  $^{15}\text{N}(\text{Leu})\text{--}^{15}\text{N}(\text{Phe}) = 2.83 \text{ \AA}$ .

The experiment uses a rather long mixing period for transferring coherence between the  $^{15}\text{N}$  nuclei. However, T-MREV is a  $\gamma$ -encoded multiple-pulse recoupling scheme. Since  $\gamma$ -encoded recoupling displays only a weak dependence on the azimuthal powder angle  $\gamma_{\text{CR}}$  (43) which corresponds to a rotation around the rotor axis, rotor synchronization is expected to have only a minor influence on the dephasing data. In a similar experiment, Tycko and co-workers (37, 38) showed that anisotropic polarization transfer affects the extracted angle in the limit of incomplete magnetization transfer. In our experiments, a mixing time of 3.98 s was used, at which time the transfer between neighboring residues has reached a plateau. We therefore assume an isotropic model in approximating the polarization transfer dynamics, noting that precise description of this process would require further knowledge of the nearby proton geometry (33–35). However, even for the case in which the polarization transfer is assumed to be purely anisotropic, significant perturbation of the dephasing trajectory is expected

only when the  $\text{N}_i\text{--N}_{i+1}$  vector is nearly colinear with  $\text{H}_i\text{--N}_i$  or  $\text{H}_{i+1}\text{--N}_{i+1}$  (51). Such near linearity occurs only with nonstandard peptide geometry ( $-50^\circ < \psi < 10^\circ$ ,  $90^\circ < \phi < 150^\circ$ ). Even in this unrealistic case, the angle would be perturbed by not more than  $\pm 5^\circ$  due to the inadequacies of the polarization transfer model. Over the majority of the Ramachandran space this effect is negligible in comparison to other experimental errors.

The proposed experiment is the first to use  $\gamma$ -encoded recoupling over multiple rotor periods to correlate dipolar interaction for structure determination. Reintroduction of the heteronuclear dipolar interaction over multiple rotor periods is in general desirable, since this allows analysis of the long-term behavior of the dephasing signal which emphasizes weaker couplings. Thus, a more accurate determination of the relative orientation of the dipolar interaction tensors is possible. Ishii *et al.* (17, 52) used the RHEDS sequence (rotor-synchronous heteronuclear dipolar switching) to correlate a NH and a CH dipolar dephasing period over multiple rotor periods in separate dimensions. The RHEDS sequence combines the WIM-12 (53) and FSLG-2 (54) multiple-pulse sequences to accumulate phase over several rotor periods. However, this sequence is not  $\gamma$ -encoded, and the dipolar scaling factor is smaller by a factor of 2.24 than the fivefold T-MREV sequence. Further analysis of the dephasing data obtained by the RHEDS sequence may be complicated by the combination of two multiple-pulse mixing sequences; in particular, correct accounting for differential relaxation would require analyzing the relative performance of the two pulse sequences. The experiments presented previously (39) demonstrate the value of considering differential relaxation for highly accurate  $^{15}\text{N}\text{--}^1\text{H}$  distance measurements.

## CONCLUSION

We have shown that correlation of two NH vectors in the peptide backbone can provide valuable information for the determination of structure in uniformly  $^{15}\text{N}$ -labeled samples. We have demonstrated that the  $\text{NH}_i\text{--NH}_{i+1}$  projection angle  $\theta_{i,i+1}$  can be measured to constrain  $\phi_i$  and  $\psi_i$  in a peptide backbone with high accuracy. The method does not rely on  $^{13}\text{C}$  labeling of the peptide. The results agree with other solid-state NMR experiments which determine these torsion angles individually (55). This type of information cannot easily be obtained in liquid-state NMR experiments due to the inherently smaller interactions. In addition, we used a  $\gamma$ -encoded recoupling sequence to reintroduce the heteronuclear dipolar interaction over multiple rotor periods in a tensor correlation experiment, where the heteronuclear dipolar interaction is not refocused after each rotor period. Precise calibration of the absolute value of the dipolar scaling factor of the sequence is not crucial for extracting the projection angle restraints. We provide a quasi-analytical formalism for the evaluation of the data, and expect this method to become extremely valuable for

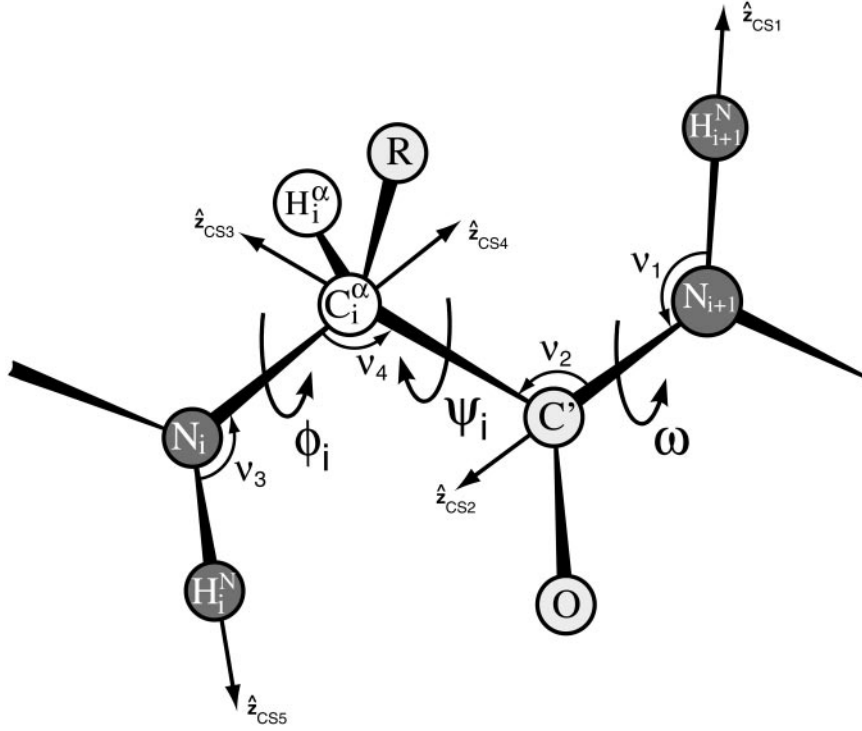


**FIG. A1.** Protein backbone showing the relevant angles and coordinate system axis for the Wigner rotations described in the text.

the determination of the relative orientation of adjacent secondary structure elements in larger spin systems.

### APPENDIX

The projection angle between the two vectors  $N_{i+1}-H_{i+1}$  and  $N_i-H_i$  can be expressed as a function of the backbone angles  $\phi_i$  and  $\psi_i$  using several sequential Wigner rotations (56). The Wigner matrix  $\tilde{\mathbf{R}}(\alpha, \beta, \gamma)$  describes a general rotation of a coordinate system according to the Euler angles  $\alpha$ ,  $\beta$ , and  $\gamma$ :

$$\tilde{\mathbf{R}}(\alpha, \beta, \gamma) = \begin{pmatrix} c\alpha \cdot c\beta \cdot c\gamma - s\alpha \cdot s\gamma & & & \\ -c\alpha \cdot c\beta \cdot s\gamma - s\alpha \cdot c\gamma & & & \\ c\alpha \cdot s\beta & & & \\ s\alpha \cdot c\beta \cdot c\gamma + c\alpha \cdot s\gamma & -s\beta \cdot c\gamma & & \\ -s\alpha \cdot c\beta \cdot s\gamma + c\alpha \cdot c\gamma & s\beta \cdot s\gamma & & \\ s\alpha \cdot s\beta & c\beta & & \end{pmatrix}. \quad [\text{A1}]$$

The original coordinate system CS1 is characterized with the  $N_{i+1}-H_{i+1}$  parallel to the  $z_{\text{CS1}}$  axis, and the  $x$  axis within the  $H_{i+1}-N_{i+1}-C'_i$  plane (Fig. A1).

In the first step, the vector  $N_{i+1}-H_{i+1}$  is represented in a coordinate system CS2, in which the  $z_{\text{CS2}}$  axis is oriented along the  $N_{i+1}-C'_i$  axis and the  $x$  axis within the  $H_{i+1}-N_{i+1}-C'_i$  plane. In the CS2 system, the vector  $N_{i+1}-H_{i+1}$  can be expressed as a function of the bond angle  $\nu_1$  after application of a Wigner transformation

$$\tilde{\mathbf{R}}(\alpha, \beta, \gamma) = \tilde{\mathbf{R}}(0, -\nu_1, 0)^{\text{CS1} \rightarrow \text{CS2}} \quad [\text{A2}]$$

$$[N_{i+1}-H_{i+1}]^{\text{CS2}} = \tilde{\mathbf{R}}(0, -\nu_1, 0)^{\text{CS1} \rightarrow \text{CS2}} [N_{i+1}-H_{i+1}]^{\text{CS1}}. \quad [\text{A3}]$$

In this case,  $\alpha, \gamma = 0$ , and the rotation of the coordinate systems can be achieved by a change of the  $z$  axis.  $\nu_1$  was substituted for  $\beta$  and refers to the bond angle  $H_{i+1}-N_{i+1}-C'_i$ . In the second step, the coordinate system CS2 is rotated around its old  $z_{\text{CS2}}$  axis by the peptide bond torsion angle  $\omega$ , and further around its intermediate  $y$  axis by the bond angle  $\nu_2$ . The new  $z_{\text{CS3}}$  axis is now oriented along the  $C'_i-C_i^\alpha$  bond. In the coordinate system CS3, the vector  $H_{i+1}-N_{i+1}$  can be represented as

$$[N_{i+1}-H_{i+1}]^{\text{CS3}} = \tilde{\mathbf{R}}(\omega, \nu_2 - \pi, 0)^{\text{CS2} \rightarrow \text{CS3}} \times \tilde{\mathbf{R}}(0, -\nu_1, 0)^{\text{CS1} \rightarrow \text{CS2}} [N_{i+1}-H_{i+1}]^{\text{CS1}}. \quad [\text{A4}]$$

The same principles apply to the vector  $N_i-H_i$ . To represent  $N_i-H_i$  in the coordinate system CS3, the CS5 has to be rotated first by the bond angle  $\nu_3$  into CS4. Subsequently, CS4 is rotated by the torsion angle  $\pi - \phi$  around its original  $z_{\text{CS4}}$  axis, and then around the intermediate  $y$  axis according to the bond angle  $\nu_4$ . Finally, CS4 is rotated by the torsion angle  $\psi$  around the new  $z_{\text{CS3}}$  axis. This can be represented as

$$[\mathbf{N}_i-\mathbf{H}_i]^{CS3} = \tilde{\mathbf{R}}(-\phi, -\nu_4, -\psi)^{CS4 \rightarrow CS3} \\ \times \tilde{\mathbf{R}}(0, -\nu_3, 0)^{CS5 \rightarrow CS4} [\mathbf{N}_i-\mathbf{H}_i]^{CS5}. \quad [\text{A5}]$$

The projection angle  $\theta_{i,i+1}$  between  $\mathbf{N}_{i+1}-\mathbf{H}_{i+1}$  and  $\mathbf{N}_i-\mathbf{H}_i$  is thus expressed by the scalar product

$$\cos \theta_{i,i+1} = \frac{1}{d^2} [\mathbf{N}_i-\mathbf{H}_i]^{CS3} \cdot [\mathbf{N}_{i+1}-\mathbf{H}_{i+1}]^{CS3} \\ = -[\cos(\nu_1)\cos(\nu_2) + \sin(\nu_1)\sin(\nu_2)\cos(\omega)] \\ \times [\cos(\nu_3)\cos(\nu_4) + \sin(\nu_3)\sin(\nu_4)\cos(\phi)] \\ - [\sin(\nu_1)\cos(\nu_2)\cos(\omega) - \cos(\nu_1)\sin(\nu_2)] \\ \times [-\sin(\nu_3)\cos(\nu_4)\cos(\phi)\cos(\psi) \\ + \cos(\nu_3)\sin(\nu_4)\cos(\psi) \\ + \sin(\nu_3)\sin(\phi)\sin(\psi)] \\ - \sin(\nu_1)\{\cos(\nu_3)\sin(\nu_4)\sin(\psi) \\ - \sin(\nu_3)[\sin(\phi)\cos(\psi) \\ + \cos(\nu_4)\cos(\phi)\sin(\psi)]\}\sin[\omega], \quad [\text{A6}]$$

where  $d$  corresponds to the length of the  $\mathbf{N}_k-\mathbf{H}_k$  vectors.

Typical values for  $\nu_i$  are  $\nu_1 = 119.5^\circ$ ,  $\nu_2 = 115.6^\circ$ ,  $\nu_3 = 118.2^\circ$ , and  $\nu_4 = 111.0^\circ$  and  $\omega = 180^\circ$  (57). Using these values leads to Eq. [14].

## ACKNOWLEDGMENTS

This research was supported by the NIH under Grants GM-23403 and RR-00995. B.R. acknowledges support from the Deutsche Forschungsgemeinschaft (Grant Re 1435/1-1). C.P.J. is a recipient of a NSF Predoctoral Fellowship. C.M.R. was a Howard Hughes Medical Institute Predoctoral Fellow.

## REFERENCES

1. R. G. Griffin, Dipolar recoupling in MAS spectra of biological solids, *Nat. Struct. Biol.* **5**, 508–512 (1998).
2. D. P. Raleigh, M. H. Levitt, and R. G. Griffin, Rotational resonance in solid state NMR, *Chem. Phys. Lett.* **146**, 71–76 (1988).
3. M. H. Levitt, D. P. Raleigh, F. Creuzet, and R. G. Griffin, Theory and simulations of homonuclear spin pair systems in rotating solids, *J. Chem. Phys.* **92**, 6347–6364 (1990).
4. F. Creuzet, A. McDermott, R. Gebhard, K. Vanderhoef, M. B. Spjkerassink, J. Herzfeld, J. Lugtenburg, M. H. Levitt, and R. G. Griffin, Determination of membrane-protein structure by rotational resonance NMR—Bacteriorhodopsin, *Science* **251**, 783–786 (1991).
5. L. K. Thompson, A. E. McDermott, J. Raap, C. M. Vanderwielen, J. Lugtenburg, J. Herzfeld, and R. G. Griffin, Rotational resonance NMR-study of the active site in bacteriorhodopsin—Conformation of the Schiff-base linkage, *Biochemistry* **34**, 7931–7938 (1992).
6. A. E. McDermott, F. Creuzet, R. Gebhard, K. Vanderhoef, M. H. Levitt, J. Herzfeld, J. Lugtenburg, and R. G. Griffin, Determination of the internuclear distances and the orientation of functional groups by solid-state NMR—Rotational resonance study of the conformation of retinal in bacteriorhodopsin, *Biochemistry* **33**, 6129–6136 (1994).
7. A. E. McDermott, F. Creuzet, R. G. Griffin, L. E. Zawadzke, Q. Z. Ye, and C. T. Walsh, Rotational resonance determination of the structure of an enzyme-inhibitor complex—Phosphorylation of an (aminoalkyl)phosphonate inhibitor of D-alanyl-D-alanine ligase by ATP, *Biochemistry* **29**, 5767–5775 (1990).
8. P. T. Lansbury, Jr., P. R. Costa, J. M. Griffiths, E. J. Simon, M. Auger, K. Halverson, D. A. Kocisko, A. S. Hendsch, T. T. Ashburn, R. G. S. Spenser, B. Tidor, and R. G. Griffin, Structural model for the  $\beta$ -amyloid fibril based on interstrand alignment of an antiparallel-sheet comprising a C-terminal peptide, *Nat. Struct. Biol.* **2**, 990–998 (1995).
9. T. L. S. Benzinger, D. M. Gregory, T. S. Burkoth, H. Miller-Auer, G. G. Lynn, R. E. Botto, and S. C. Meredith, Propagating structure of Alzheimer's  $\beta$ -amyloid(10-35) is parallel beta-sheet with residues in exact register, *Proc. Natl. Acad. Sci. USA* **95**, 13407–13412 (1998).
10. T. Gullion and J. Schaefer, Rotational-echo-double-resonance NMR, *J. Magn. Reson.* **81**, 196–200 (1989).
11. V. Copie, A. C. Kolbert, D. H. Drewry, P. A. Barlett, T. G. Oas, and R. G. Griffin, Inhibition of thermolysin by phosphoramidate transition-state analogs—Measurement of  $^{31}\text{P}$ - $^{15}\text{N}$  bond lengths and chemical shifts in 2 enzyme-inhibitor complexes by solid-state nuclear-magnetic-resonance, *Biochemistry* **29**, 9176–9184 (1990).
12. L. M. McDowell, C. A. Klug, D. D. Beusen, and J. Schaefer, Ligand geometry of the ternary complex of 5-enolpyruvylshikimate-3-phosphate synthase from rotational-echo double-resonance NMR, *Biochemistry* **35**, 5395–5403 (1996).
13. D. R. Studelska, L. M. McDowell, M. P. Espe, C. A. Klug, and J. Schaefer, Slowed enzymatic turnover allows characterization of intermediates by solid-state NMR, *Biochemistry* **36**, 15555–15560 (1997).
14. K. Schmidt-Rohr, Torsion angle determination in solid  $^{13}\text{C}$ -labeled amino acids and peptides by separated-local-field double-quantum NMR, *J. Am. Chem. Soc.* **118**, 7601–7603 (1996).
15. X. Feng, T. K. Lee, D. Sandstrom, M. Edén, H. Maisel, A. Sebald, and M. H. Levitt, Direct determination of a molecular torsional angle by solid-state NMR, *Chem. Phys. Lett.* **257**, 314–320 (1996).
16. M. Hong, J. D. Gross, and R. G. Griffin, Site-resolved determination of peptide torsion angle  $\phi$  from the relative orientation of backbone N–H and C–H bonds by solid-state NMR, *Phys. Chem. B* **101**, 5869–5874 (1997).
17. Y. Ishii, K. Hirao, T. Terao, T. Terauchi, M. Oba, N. Nishiyama, and M. Kainosho, Determination of peptide  $\phi$  angles in solids by relayed anisotropy correlation NMR, *Solid State Nucl. Magn. Reson.* **11**, 169–175 (1998).
18. X. Feng, M. Edén, A. Brinkmann, H. Luthman, L. Eriksson, A. Graslund, O. N. Antzutkin, and M. H. Levitt, Direct determination of a peptide torsional angle  $\psi$  by double-quantum solid-state NMR, *J. Am. Chem. Soc.* **119**, 12006–12007 (1997).
19. P. R. Costa, J. D. Gross, M. Hong, and R. G. Griffin, Solid-state NMR Measurement of  $\psi$  in peptides: A NCCN 2Q-heteronuclear local field experiment, *Chem. Phys. Lett.* **280**, 95–103 (1997).
20. T. Fujiwara, T. Shimomura, Y. Ohigashi, and H. Akutsu, Multidimensional solid-state nuclear magnetic resonance for determining the dihedral angle from the correlation of  $^{13}\text{C}$ - $^1\text{H}$  and  $^{13}\text{C}$ - $^{13}\text{C}$  dipolar interactions under magic-angle spinning conditions, *J. Chem. Phys.* **109**, 2380–2393 (1998).
21. P. R. Costa, "Spins, Peptides, and Alzheimer's Disease: Solid-

- State Nuclear Magnetic Resonance of Amyloid Peptide Conformation," Ph.D. Thesis, Massachusetts Institute of Technology (1996).
22. M. Hohwy, C. M. Rienstra, C. P. Jaroniec, and R. G. Griffin, Fivefold symmetric homonuclear dipolar recoupling in rotating solids: Application to double quantum spectroscopy, *J. Chem. Phys.* **110**, 7983–7992 (1999).
  23. P. Hodgkinson and L. Emsley, The accuracy of distance measurements in solid-state NMR, *J. Magn. Reson.* **139**, 46–59 (1999).
  24. K. Takegoshi, K. Nomura, and T. Terao, Rotational resonance in the tilted rotating-frame, *Chem. Phys. Lett.* **232**, 424–428 (1995).
  25. K. Takegoshi, K. Nomura, and T. Terao, Selective homonuclear polarization transfer in the tilted rotating frame under magic angle spinning in solids, *J. Magn. Reson.* **127**, 206–216 (1997).
  26. P. R. Costa, B. Q. Sun, and R. G. Griffin, Rotational resonance tickling: Accurate internuclear distance measurement in solids, *J. Am. Chem. Soc.* **119**, 10821–10830 (1997).
  27. K. Nomura, K. Takegoshi, T. Terao, K. Uchida, and M. Kainosho, Determination of the complete structure of a uniformly labeled molecule by rotational resonance solid-state NMR in the tilted rotating frame, *J. Am. Chem. Soc.* **121**, 4064–4065 (1999).
  28. C. A. Michal and L. W. Jelinski, REDOR 3D: Heteronuclear distance measurement in uniformly labeled and natural abundance solids, *J. Am. Chem. Soc.* **119**, 9050–9060 (1997).
  29. T. Gullion and C. H. Pennington,  $\theta$ -REDOR: A MAS NMR method to simplify multiple coupled heteronuclear spin systems, *Chem. Phys. Lett.* **290**, 89–93 (1998).
  30. J. Schaefer, REDOR-determined distances from heterospins to clusters of  $^{13}\text{C}$  labels, *J. Magn. Reson.* **137**, 272–275 (1999).
  31. C. P. Jaroniec, B. A. Tounge, C. M. Rienstra, J. Herzfeld, and R. G. Griffin, Measurement of  $^{13}\text{C}$ - $^{15}\text{N}$  distances in uniformly  $^{13}\text{C}$  labeled biomolecules: *J*-decoupled REDOR, *J. Am. Chem. Soc.* **121**, 10237–10238 (1999).
  32. H. J. Showell, R. J. Freer, S. H. Zigmond, E. Schiffmann, S. Aswanikumar, B. Corcoran, and E. L. Becker, The structure-activity relations of synthetic peptides as chemotactic factors and inducers of lysosomal secretion for neutrophils, *J. Exp. Med.* **143**, 1154–1169 (1976).
  33. D. Suter and R. R. Ernst, Spectral spin diffusion in the presence of an extraneous dipolar reservoir, *Phys. Rev. B* **25**, 6038–6041 (1982).
  34. D. Suter and R. R. Ernst, Spin diffusion in resolved solid-state NMR spectra, *Phys. Rev. B* **32**, 5608–5627 (1985).
  35. A. Kubo and C. A. McDowell, Spectral spin diffusion in polycrystalline solids under magic angle spinning, *J. Chem. Soc. Faraday Trans. 1* **84**, 3713–3730 (1988).
  36. G. Dabbagh, D. P. Weliky, and R. Tycko, Determination of monomer conformation in noncrystalline solid polymers by 2-dimensional NMR exchange spectroscopy, *Macromolecules* **27**, 6183 (1994).
  37. D. P. Weliky and R. Tycko, Determination of peptide conformations by two-dimensional magic angle spinning NMR exchange spectroscopy with rotor synchronization, *J. Am. Chem. Soc.* **118**, 8487–8488 (1996).
  38. R. Tycko, D. P. Weliky, and A. E. Berger, Investigation of molecular structure in solids by two-dimensional NMR exchange spectroscopy with magic angle spinning, *J. Chem. Phys.* **105**, 7915–7930 (1996).
  39. M. Hohwy, C. P. Jaroniec, B. Reif, C. M. Rienstra, and R. G. Griffin, Local structure and relaxation in solid-state NMR: Accurate measurement of amide N–H bond lengths and H–N–H bond angles, *J. Am. Chem. Soc.* **122**, 3218–3219 (2000).
  40. P. Mansfield, M. J. Orchard, D. C. Stalker, and K. H. B. Richards, Symmetrized multipulse nuclear-magnetic-resonance experiments in solids: Measurement of the chemical-shift shielding tensor in some compounds, *Phys. Rev. B* **7**, 90–105 (1973).
  41. W. K. Rhim, D. D. Elleman, and R. W. Vaughan, Analysis of multiple-pulse NMR in solids, *J. Chem. Phys.* **59**, 3740–3749 (1973).
  42. W. K. Rhim, D. D. Elleman, L. B. Schreiber, and R. W. Vaughan, Analysis of multiple pulse NMR in solids. II, *J. Chem. Phys.* **60**, 4595–4604 (1974).
  43. N. C. Nielsen, H. Bildsøe, H. J. Jacobsen, and M. H. Levitt, Double-quantum homonuclear rotary resonance: Efficient dipolar recovery in magic-angle spinning nuclear magnetic resonance, *J. Chem. Phys.* **101**, 1805–1812 (1994).
  44. J. D. Gross, P. R. Costa, and R. G. Griffin, Tilted *n*-fold symmetric radio frequency pulse sequences: Applications to CSA and heteronuclear dipolar recoupling in homonuclear dipolar coupled spin networks, *J. Chem. Phys.* **108**, 7286–7293 (1998).
  45. H. W. Spiess, "NMR Basic Principles and Progress," Springer-Verlag, Berlin (1978).
  46. Y. K. Lee, N. D. Kurur, M. Helmle, O. G. Johannessen, N. C. Nielsen, and M. H. Levitt, Efficient dipolar recoupling in the NMR of rotating solids. A sevenfold symmetric radiofrequency pulse sequence, *Chem. Phys. Lett.* **242**, 304–309 (1995).
  47. Reference deleted in proof.
  48. M. G. Munowitz and R. G. Griffin, Two dimensional nuclear magnetic resonance in rotating solids: An analysis of line shapes in chemical shift-dipolar spectra, *J. Chem. Phys.* **76**, 2848–2858 (1982).
  49. A. E. Bennett, C. M. Rienstra, M. Auger, K. V. Lakshmi, and R. G. Griffin, Heteronuclear decoupling in rotating solids, *J. Chem. Phys.* **103**, 6951–6958 (1995).
  50. E. Gavuzzo, F. Mazza, G. Pochetti, and A. Scatturin, Crystal structure, conformation, and potential energy calculations of the chemotactic peptide *N*-formyl-L-Met-L-Leu-L-Phe-OME, *Int. J. Peptide Protein Res.* **34**, 409–415 (1989).
  51. C. M. Rienstra, "Solid State Nuclear Magnetic Resonance Methodology for Biomolecular Structure Determination," Ph.D. Thesis, Massachusetts Institute of Technology (1999).
  52. Y. Ishii, T. Terao, and M. Kainosho, Relayed anisotropy correlation NMR: Determination of dihedral angles in solids, *Chem. Phys. Lett.* **256**, 133–140 (1996).
  53. P. Caravatti, L. Braunschweiler, and R. R. Ernst, Heteronuclear correlation spectroscopy in rotating solids, *Chem. Phys. Lett.* **100**, 305–310 (1983).
  54. A. Bielecki, A. C. Kolbert, and M. H. Levitt, Frequency-switched pulse sequences—Homonuclear decoupling and dilute spin NMR in solids, *Chem. Phys. Lett.* **155**, 341–346 (1989).
  55. C. M. Rienstra, M. Hohwy, L. Mueller, M. Hong, C. Jaroniec, B. Reif, and R. G. Griffin, 40th Experimental NMR Conference (ENC), Orlando, FL (1999).
  56. K. Schmidt-Rohr and H. W. Spiess, "Multidimensional Solid-State NMR and Polymers," Academic Press, London (1994).
  57. T. E. Creighton, "Proteins: Structures and Molecular Properties," 2nd ed., Freeman, New York (1993).